CrossMark

J. Plasma Phys. (2020), *vol*. 86, 905860514 © The Author(s), 2020.
Published by Cambridge University Press
doi:10.1017/S0022377820001178

Stability of a tokamak plasma with diffuse toroidal rotation

O. E. López [1],† **and L. Guazzotto** [1]

[1]Physics Department, Auburn University, Auburn, AL 36849, USA

(Received 5 May 2020; revised 28 August 2020; accepted 2 September 2020)

The present work considers the stability of a high-β, large aspect ratio, circular plasma with diffuse profiles for the safety factor and the angular toroidal frequency (López & Guazzotto, *Phys. Plasmas*, vol. 24, 032501). An application of the Frieman–Rotenberg formalism results in a system of scalar eigenmode equations whose coupling is retained at the plasma–vacuum transition but is disregarded across the plasma column, which is a standard practice. The solution technique consists of a multidimensional shooting method for the poloidal harmonics; robust initial guesses are constructed by solving the dispersion relation in the static scenario with vanishing magnetic shear. Flow shear appears as a high-β toroidal contribution, and we illustrate its destabilizing influence on $n = 1$ external kink modes in the presence of ideal and resistive walls. Internal resonances are avoided by means of the selection of appropriate equilibrium parameters. The stabilizing influence of a finite positive average magnetic shear is also exemplified.

Key words: plasma flows, fusion plasma, plasma instabilities

1. Introduction

Magnetically confined plasmas can display significant rotation levels throughout standard machine operation. For example, a deuterium plasma has reached toroidal velocities of approximately 40 % the sound speed in the DIII-D tokamak (Baylor *et al.* 2004, figure 9) and the National Spherical Torus Experiment (NSTX) has reported toroidal velocities of approximately half the Alfvén speed (Sabbagh *et al.* 2006, p. 641). Rotation is typically induced by neutral beam injection (known as NBI) or radio-frequency (known as RF) heating (Suckewer *et al.* 1981; Eriksson, Righi & Zastrow 1997).

There is a tradition of analytical and numerical magneto-hydro-dynamics (MHD) studies that aim at determining the stability consequences of the presence of toroidal flows. To cite but a few, studies include the effect of flow or flow shear on interchange modes (Chu 1998; Wahlberg & Bondeson 2001) and on ballooning modes (Cooper 1988; Waelbroeck & Chen 1991), toroidal rotation effects on internal modes (Waelbroeck 1996; Wahlberg & Bondeson 2000; Wahlberg, Chapman & Graves 2009) and on resistive wall modes (Bondeson & Ward 1994; Betti & Freidberg 1995; Chu *et al.* 1995; Fitzpatrick & Aydemir 1996; Betti 1998), etc. The destabilizing influence of flow shear due to a Kelvin–Helmholtz effect has also been recognized (Chandrasekhar 1961; Chapman *et al.* 2011, 2012; Wahlberg, Graves & Chapman 2013; Brunetti, Lazzaro & Nowak 2017), and

† Email address for correspondence: oelopez@auburn.edu

https://doi.org/10.1017/S0022377820001178 Published online by Cambridge University Press

has been studied by the spectral web method (Goedbloed, Keppens & Poedts 2010). Conversely, numerical studies indicate that flow shear can stabilize ideal external kink modes in fast-rotating spherical tokamaks (Chapman *et al.* 2011) as well as sausage and kink modes in a Z-pinch (Shumlak & Hartman 1995).

This work focuses on the effect of flow shear on the stability of external modes. External kink modes constitute one of the most serious MHD instabilities in tokamaks due to the fact that they impose limits on the plasma β (the ratio between the kinetic pressure and the magnetic pressure). Interestingly, numerical computations have found that flow shear can increase the (no wall) ideal external kink stability limit (Chapman *et al.* 2011) with the caveat that if the rotation speed approaches a significant fraction of the Alfvén speed (V_{Ao}), a Kelvin–Helmholtz mode might be driven unstable (Chapman *et al.* 2011, 2012). Given characteristic values for the vacuum magnetic field ($B_{\varphi o}$) and mass density (ρ_o), the Alfvén velocity is $V_{\mathrm{Ao}} = B_{\varphi o}/\sqrt{\mu_o \rho_o}$, here, μ_o is the permeability of free space. The theory developed in Chapman *et al.* (2011) assumes a toroidal rotation of the order $V_\varphi \sim \epsilon V_A$, and a low-$\beta$ plasma ($\beta \sim \epsilon^2$). As usual, the inverse aspect ratio is defined as $\epsilon = a/R_o$, where a and R_o are the minor radius and the major radius for the configuration, respectively. In Chapman *et al.* (2011) it is demonstrated that there exist windows of stability against ideal external kink modes and the Kelvin–Helmholtz instability, which may be relevant for the operation of fast-rotating plasmas in spherical tokamaks. Further numerical and analytical calculations for low-β configurations with strongly sheared toroidal flows have extended these results (Wahlberg *et al.* 2013). In this work, the investigation of external kink modes and flow shear is continued for high-β plasmas; however, rather than exploring scenarios with strong variations in the flow profile, the focus is on mild flow shear effects. While Chapman *et al.* (2011) assume that temperature is constant on flux surfaces, and there is an associated centrifugal redistribution of the mass density and of the pressure, the present work considers adiabatic plasmas. In this work, it is found that flow shear is always destabilizing. Additionally, it is shown that a positive average magnetic shear has a stabilizing influence on the plasma column, and that this stabilizing effect is stronger at low values for the plasma β.

It has been observed that failure to self-consistently incorporate the effect of flow at the equilibrium level can lead to dissimilar stability conclusions 'even at modest flows speeds' (Wahlberg *et al.* 2009). Accordingly, our stability calculations have been built upon a high-β analytic equilibrium with diffuse profiles in the safety factor and in the angular toroidal frequency. This equilibrium has been developed for a large aspect ratio plasma (López & Guazzotto 2017). For the purposes of modelling realistic high-β fast rotating plasmas, as in NSTX, it would be important to incorporate cross-sectional shaping, as done in (Chapman *et al.* 2011, 2012). Despite the fact that an analytic D-shaped equilibrium solution for a flowing plasma has been constructed in López & Guazzotto (2017), the present stability analysis is limited to circular cross-sections. In addition, even if the safety factor is divergent in configurations with a separatrix, we consider scenarios without internal resonances; this restriction could be relaxed in future work. On the other hand, the effect of ideal and resistive walls has been taken into account. An application of the Frieman–Rotenberg formalism, in combination with the formulation developed by Betti (1998), allowed us to reduce the linear stability problem to an eigenvalue system of scalar differential equations (ODEs). We have solved these equations by employing a multidimensional shooting method and a robust technique to compute initial guesses nearby the fastest-growing modes has been developed. Interestingly, flow shear constitutes a new high-β toroidal effect that disappears in the cylindrical limit. The fact that centrifugal and Coriolis effects have been ordered out in our model, has allowed us to isolate the effect of flow shear. We illustrate that variations in the wall position for marginal

https://doi.org/10.1017/S0022377820001178 Published online by Cambridge University Press

stability due to flow shear may be of the same order of magnitude as those experienced when the plasma possesses a comparable rigid toroidal angular frequency. The text is organized as follows. Section 2 introduces the equilibrium configuration in the plasma column. The equilibrium configuration in the vacuum region is determined in § 3. The Frieman–Rotenberg formalism is summarized in § 4, and a form of the spectral equation for axisymmetric configurations is derived there. The Shear–Alfvén law is presented in § 5. The stability problem is reduced to an eigenvalue system of scalar ODEs in § 6. Appropriate boundary conditions and material wall effects are considered in § 7, but mathematical details are provided in appendix B. A shooting method implementation for the stability problem is explained in § 8. Marginal stability curves and characteristic growth rates under different scenarios are presented in § 9. A summary and discussion are provided in § 10. In order to deal with the singular nature of the governing ODEs in the stability analysis, a new series-form equilibrium solution is constructed in appendix A.

2. Equilibrium model: plasma column

We consider a plasma of mass density ρ, kinetic pressure p, rotating toroidally with angular frequency Ω, and under the influence of a magnetic field $\boldsymbol{B}$. The aim of this article is to explore finite flow shear effects on linear stability. The equilibrium under consideration possesses mild, global velocity gradients ($\nabla\Omega \sim \Omega/a$) across the plasma column. This is to be contrasted with scenarios with localized toroidal flow shear (Lee & Cerfon 2019).

The configuration of interest consists of a toroidally rotating plasma (of radius a) bounded by a thin resistive wall (located at $r = r_w$) of thickness d and resistivity η_w. There are two vacuum regions: an inner region ($a < r < r_w$) and an outer one ($r > r_w$). Throughout this work, we employ the right-handed cylindrical system (R, φ, Z), where Z is the symmetry axis and φ the ignorable coordinate; as well as the right-handed, chamber-centred coordinate system (r, φ, θ).

At equilibrium, the momentum equation is

$$\nabla\left(p + \frac{B^2}{2\mu_o}\right) = \frac{1}{\mu_o}\boldsymbol{B}\cdot\nabla\boldsymbol{B} + \rho\Omega^2 R\nabla R. \tag{2.1}$$

As is well known, the MHD axisymmetric equilibrium problem with macroscopic flows in an arbitrary direction reduces to the Grad–Shafranov–Bernoulli (GSB) system of equations. It is obtained from the MHD equations for mass and momentum conservation in addition to Maxwell's equations and an appropriate closure equation (Hameiri 1983). For purely toroidally rotating plasmas,

$$\boldsymbol{V} = R\Omega(\Psi)\hat{\boldsymbol{e}}_\varphi, \tag{2.2}$$

where $\hat{\boldsymbol{e}}_\varphi$ is the unitary vector in the toroidal direction, the GSB system can be cast as

$$\frac{1}{\mu_o}\nabla\cdot\left[\frac{\nabla\Psi}{R^2}\right] = -\frac{B_\varphi F'(\Psi)}{\mu_o R} - \rho R V_\varphi \Omega'(\Psi) - \rho H'(\Psi) + \frac{\rho^\gamma}{\gamma-1}S'(\Psi), \tag{2.3}$$

$$\rho H(\Psi) = \frac{\gamma p}{\gamma-1} + \frac{1}{2}\rho V_\varphi^2. \tag{2.4}$$

For a given set of free functions: $F(\Psi)$, $\Omega(\Psi)$, $S(\Psi)$ and $H(\Psi)$, and boundary conditions, the GSB equations are simultaneously solved for the magnetic poloidal flux ($\Psi =$

https://doi.org/10.1017/S0022377820001178 Published online by Cambridge University Press

$\Psi(R, Z)$) and the plasma mass density ($\rho = \rho(R, Z)$). The magnetic field is obtained from

$$\boldsymbol{B} = \nabla\Psi \times \nabla\varphi + F(\Psi)\nabla\varphi. \tag{2.5}$$

In this formulation, the kinetic pressure is not a flux quantity, instead, it is obtained from the MHD closure equation for isentropic flows,

$$p = S(\Psi)\rho^{\gamma}, \tag{2.6}$$

where γ is the adiabatic constant. For an ideal gas $\gamma = 5/3$, the isothermal case is recovered as γ approaches unity.

In López & Guazzotto (2017), a self-consistent, high-β tokamak equilibrium solution for a circular plasma with toroidal and poloidal flows is developed as an asymptotic expansion of the complete GSB system in terms of the inverse aspect ratio. In this work, we utilize a reduced version of this equilibrium solution, where poloidal flows are set equal to zero, as our starting point. This is a reasonable assumption in view of the ion–ion collision damping for the poloidal flow (Hassam & Kulsrud (1978); Hinton & Wong (1985); Catto, Bernstein & Tessarotto (1987); Morris, Haines & Hastie (1996), to cite some). In the remainder of this section, we summarize and further develop those parts of the equilibrium introduced by López & Guazzotto (2017) that are relevant for the stability analysis this work focuses on.

Free functions are chosen to be the polynomials,

$$\Omega(\Psi) = \Omega_o \frac{\Psi}{a^2 B_{\varphi o}}, \tag{2.7}$$

$$S(\Psi) = \frac{\epsilon V_{Ao}^2}{\rho_o^{\gamma-1}} \left(s_0 \frac{\Psi}{a^2 B_{\varphi o}} + \epsilon \left(s_1 \frac{\Psi}{a^2 B_{\varphi o}} + \frac{1}{2} s_{11} \left[\frac{\Psi}{a^2 B_{\varphi o}} \right]^2 \right) \right), \tag{2.8}$$

$$H(\Psi) = \epsilon V_{Ao} \left(h_0 \frac{\Psi}{a^2 B_{\varphi o}} + \epsilon \left(h_1 \frac{\Psi}{a^2 B_{\varphi o}} + \frac{1}{2} h_{11} \left[\frac{\Psi}{a^2 B_{\varphi o}} \right]^2 \right) \right), \tag{2.9}$$

$$F(\Psi) = R_o B_{\varphi o} \left(f_0 + \epsilon \left(f_1 \frac{\Psi}{a^2 B_{\varphi o}} \right) + \epsilon^2 \left(f_2 \frac{\Psi}{a^2 B_{\varphi o}} + \frac{1}{2} f_{22} \left[\frac{\Psi}{a^2 B_{\varphi o}} \right]^2 \right) \right). \tag{2.10}$$

This choice is slightly more general than the one by Solov'ev (1968). Here, the free coefficients f_0, f_1, f_2, f_{22}, s_0, s_1, s_{11}, h_0, h_1 and h_{11}, are a set of dimensionless constants, all of them of $\sim O(1)$. On the other hand, the coefficient for the toroidal angular frequency (Ω_o) it is assumed to be a fraction of the Alfvén frequency (ω_A): $\Omega_o/\omega_A \sim O(\epsilon)$, where $\omega_A = V_{Ao}/R_o$. This ordering implies a high-β scenario $\langle\beta\rangle \sim O(\epsilon)$, where the poloidal magnetic field is a fraction of the toroidal one, $B_p/B_{\varphi o} \sim O(\epsilon)$, and with a kink-safety factor of $q_* \sim O(1)$. Here, the kink-safety factor is defined as

$$q_* = \frac{aB_\varphi}{R_o B_p} = \frac{2\pi a^2 B_{\varphi o}}{\mu_o R_o I}, \tag{2.11}$$

where I represents the total toroidal current and the other quantities have been defined before. An explicit expression for $\langle\beta\rangle$ is presented later on. As a boundary condition, it is required that the poloidal flux vanishes at the plasma edge,

$$\Psi(a, \theta) = 0. \tag{2.12}$$

Under these assumptions, the poloidal flux is found to have a simple closed-form analytical expression; it involves Bessel functions of the first and second kind, and the

https://doi.org/10.1017/S0022377820001178 Published online by Cambridge University Press

Meijer G-function (López & Guazzotto 2017). The solution depends on three figures of merit: the kink safety factor (q_*), which has been introduced in (2.11); a quantity that determines the β regime (ν), which is explicitly given in (2.14); and a measure for the mean magnetic shear (λ), which is implicitly defined by (2.23); the solution is expressed in the generic way,

$$\Psi\,(r,\theta) = \Psi_0(r, q_*, \lambda) + \nu\Psi_1(r, q_*, \lambda)\cos(\theta) + O(\epsilon B_{\varphi o} a^2). \tag{2.13}$$

For the convenience of readers, the equilibrium solution for the poloidal flux that was originally constructed by López & Guazzotto (2017) is provided in appendix A. In particular, Ψ_0 and Ψ_1 are given in closed form by (A 4) and (A 5), respectively. While (A 5) is a convenient analytical formula, it is observed that it is singular at $r = 0$. A new, series-form representation for Ψ_1 that alleviates this issue is presently introduced (A 6).

We emphasize that Ψ_0 and Ψ_1 are both leading-order contributions to the poloidal flux, i.e. $\Psi_0(r) \sim \Psi_1(r) \sim O(a^2 B_{\varphi o})$. Here, ν has a dual meaning: it sets the equilibrium β regime, and it acts as a coupling coefficient for the poloidal modes in the stability analysis. It is defined as

$$\nu \equiv \langle\beta\rangle q_*^2/\epsilon, \tag{2.14}$$

where $\langle\beta\rangle$ is obtained as an average over the plasma volume (V_p),

$$\langle\beta\rangle = \frac{2\mu_o\langle p\rangle}{B_{\varphi o}^2} = \frac{2\mu_o}{B_{\varphi o}^2}\frac{1}{V_p}\int p\,\mathrm{d}^3 r. \tag{2.15}$$

Despite the fact that the stationary equilibrium solution is formally derived for high-β scenarios ($\nu \sim 1$), it is possible to explore low-β configurations ($\nu \ll 1$) as well. The expression for the safety factor at the plasma surface (q_a),

$$q_a = \frac{F(\Psi)}{2\pi}\oint \frac{\mathrm{d}l}{R^2 B_p} = \frac{q_*}{\sqrt{1-\nu^2}}, \tag{2.16}$$

indicates that the equilibrium possesses the β-limit,

$$\nu < 1. \tag{2.17}$$

Another key figure of merit is the magnetic shear. This quantity measures the change of the relative orientation of field lines in neighbouring magnetic surfaces. In general, larger shear is related to better stability properties. In low-β, large aspect ratio configurations, where the poloidal flux is independent of the poloidal angle (to leading order), a simple expression for the magnetic shear is (Freidberg 2014),

$$s(r) \equiv \frac{r}{q}\frac{\mathrm{d}q}{\mathrm{d}r}, \tag{2.18}$$

(not to be confused with the entropy free function) where $q(r)$, the safety factor, is defined here as

$$q(r) \equiv \left(\frac{1}{rB_{\varphi o}}\frac{\mathrm{d}\Psi_0}{\mathrm{d}r}\right)^{-1}. \tag{2.19}$$

It was determined in López & Guazzotto (2017) that λ, which appears in (2.13), is an auxiliary variable arising during the simplification of the GSB system (see (A 1)), and that

https://doi.org/10.1017/S0022377820001178 Published online by Cambridge University Press

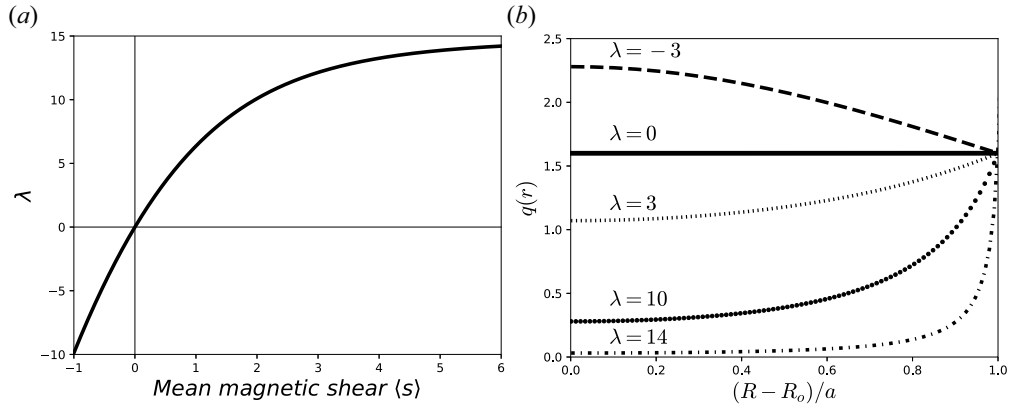


FIGURE 1. (*a*) The λ parameter as a function of the average magnetic shear ($\langle s\rangle$) in a low-β approximation. (*b*) Safety factor in a low-β scenario for varying values of λ.

it is related to the free coefficients introduced in (2.7)–(2.10) through the transcendental equation,

$$\lambda = \frac{\nu^2 f(\lambda)^2}{q_*^2 f_0^2} + \frac{\Omega_o^2}{\epsilon^2 \omega_A^2 \rho_0} + f_0 f_{22} + \rho_0 h_{11} - \frac{s_{11}\rho_0^\gamma}{\gamma - 1}, \tag{2.20}$$

here, the leading-order dimensionless density is

$$\rho_0 = \left(\frac{(\gamma-1)h_0}{\gamma s_0}\right)^{1/(\gamma-1)} \tag{2.21}$$

and

$$f(\lambda) \equiv -\frac{2J_1(\sqrt{\lambda})}{{}_0\tilde{F}_1\left(;3;-\frac{\lambda}{4}\right)\sqrt{\lambda}}, \tag{2.22}$$

where ${}_0\tilde{F}_1$ is the regularized confluent hypergeometric function (DLMF 2020, § 15.1). Interestingly, λ can be regarded as a measure of the magnetic shear. This is more easily seen by considering a low-β approximation. In that regime, the average value of the magnetic shear over the cross-section of the plasma (A_p) has a simple form,

$$\langle s\rangle \equiv \frac{1}{A_p}\int s(r)\,\mathrm{d}^2 r = 1 - 2\ln\left(J_1(\sqrt{\lambda})\right) + 4\int_0^1 \bar{r}\ln\left(J_1\left(\sqrt{\lambda}\bar{r}\right)\right)\mathrm{d}\bar{r} + O(\nu). \tag{2.23}$$

This is to be understood as an implicit definition for λ in terms of the magnetic shear: $\lambda = \lambda(\langle s\rangle)$. Figure 1(*a*) shows a monotonic dependence between $\langle s\rangle$ and λ. Positive (negative) values for the average shear correspond to positive (negative) values for λ. As the magnetic shear increases, λ approaches the squared value of a Bessel function's zero ($j_{1,1}^2 = 14.682$) asymptotically. As exemplified in figure 1(*b*) for a low-β configuration, the safety factor's concavity changes in accordance with the sign of λ, being flat when λ vanishes.

Additional quantities that will be necessary for the determination of the equilibrium configuration in the vacuum region, as well as to carry out the stability analysis, are the

https://doi.org/10.1017/S0022377820001178 Published online by Cambridge University Press

equilibrium mass density and pressure. It is possible to prove that the leading-order mass density is constant,

$$\rho(r,\theta) = \rho_o + O(\epsilon\rho_o), \tag{2.24}$$

and that the leading-order kinetic pressure is a flux quantity (López & Guazzotto 2017). A convenient representation for the pressure, which is not explicitly given by López & Guazzotto (2017), is

$$p(\Psi) = \frac{B_{\varphi o}}{\mu_o a^2}\langle\beta\rangle q_* f(\lambda)\Psi + O\left(\epsilon\langle\beta\rangle B_{\varphi o}^2/\mu_o\right), \tag{2.25}$$

where $f(\lambda)$ has been defined in (2.22). Moreover, in view of the homogeneous Dirichlet condition for the poloidal flux (2.12), it follows that both the kinetic pressure and the angular toroidal velocity vanish at the plasma edge,

$$p(a,\theta) = 0, \quad \Omega(a,\theta) = 0. \tag{2.26a,b}$$

This leads to convenient simplifications in the evaluation of the boundary conditions at the plasma–vacuum transition.

In regards to the free function $F(\Psi)$, it is evident that f_0 controls the vacuum toroidal magnetic field. The diamagnetic depression of the toroidal magnetic field (or paramagnetic response in the case, e.g. of a reversed field pinch or, possibly, an ohmic tokamak) is determined by f_1, f_2 and f_{22}. In particular, the coefficient f_1 is given by

$$f_1 = \frac{\nu f(\lambda)}{q_* f_0}. \tag{2.27}$$

It has been shown that q_*, ϵ, λ and ν define the poloidal flux (2.13). Evidently, these parameters should be related to the free coefficients introduced in (2.7)–(2.10). Indeed, (2.20) and (2.27) represent two of these relations. Additionally, it is possible to prove that the following relation holds:

$$\frac{\sqrt{\lambda}J_0(\sqrt{\lambda})}{q_* J_1(\sqrt{\lambda})} = -f_0 f_2 - \rho_0 h_1 + \frac{s_1\rho_0^\gamma}{\gamma - 1}. \tag{2.28}$$

There are many combinations of the free coefficients that lead to the same form of the poloidal flux. One might think of q_*, ϵ, λ, ν and Ω_o/ω_A as independent dimensionless parameters, and the free coefficients as being implicitly chosen to self-consistent values, albeit this choice is far from being unique. More importantly, it will be proven that the stability of a given configuration depends only on these five independent parameters. Hereafter, f_0 is set to unity without loss of generality.

3. Equilibrium model: vacuum

This section's aim is the determination of the inner equilibrium vacuum magnetic field ($\boldsymbol{B}_V$). As expected, the vacuum safety factor at the plasma edge is a relevant quantity for stability considerations. This quantity is computed by imposing the continuity of the total pressure, and that of the normal component of the magnetic field, at the plasma–vacuum transition.

While the condition for the continuity of the normal component of the magnetic field, $B_r(a,\theta) = B_{Vr}(a,\theta)$, is trivially satisfied, the condition of the continuity of the total

https://doi.org/10.1017/S0022377820001178 Published online by Cambridge University Press

pressure,

$$p(a,\theta)+\frac{B^2(a,\theta)}{2\mu_o}=\frac{B_V^2(a,\theta)}{2\mu_o}, \tag{3.1}$$

is simplified by taking into account that the kinetic pressure vanishes at the plasma edge (2.25 and 2.26*a*,*b*). The poloidal component of the vacuum magnetic field is found to be

$$B_{V\theta}^2(a)=B_\theta^2(a)+D\,(1-2\epsilon\cos\theta)+O(\epsilon^3 B_{\varphi o}^2). \tag{3.2}$$

Following Betti (1998), we have introduced the difference

$$D\equiv\frac{F_a^2(a)-F_{\rm Va}^2(a)}{R_o^2}, \tag{3.3}$$

where F_a is obtained from (2.10), $F_a\equiv F(a,\theta)=R_oB_{\varphi o}$, and the free function for the vacuum side evaluated at the interface is $F_{\rm Va}\equiv F_{\rm Va}(\Psi(a,\theta))=$ constant. It is observed that D controls the amount of surface current at the plasma–vacuum transition. In many sharp-boundary models (Freidberg & Haas 1973, 1974; Freidberg & Grossmann 1975; Betti 1998; Fitzpatrick 2008; Rhodes *et al.* 2018) surface currents originate from the finite jump in the kinetic pressure at the plasma–vacuum interface. In the present model, which possesses a pressure profile that vanishes at the plasma edge, surface currents are not needed, but can be accommodated; however, for simplicity, we consider the $D=0$ case only. Equation (3.2) may be contrasted with (12) from Betti (1998). The form for the equilibrium pressure in the latter model, $p(R)=p_o\exp[(R^2/R_o^2-1)M^2/2]$, where $M=\Omega R_o\sqrt{\rho_o/p_o}$ is the Mach number (up to a $\sqrt{3/5}$ factor), results in an extra factor, $4\epsilon\mu_o p_o(1+M^2/2)\cos\theta$, not present in (3.2).

Under these conditions, the vacuum safety factor at the plasma–vacuum transition is given by

$$q_V(a,\theta)=\frac{aB_{\varphi o}}{R_oB_{V\theta}(a,\theta)}=\frac{q_*}{1+\nu\cos\theta}. \tag{3.4}$$

Its average value at the plasma edge is

$$\langle q_V\rangle_a=\frac{1}{2\pi}\int_0^{2\pi}\frac{aB_{\varphi o}\,{\rm d}\theta}{R_oB_{V\theta}(a,\theta)}=\frac{q_*}{\sqrt{1-\nu^2}}=q_a. \tag{3.5}$$

Finally, a quantity of interest for stability considerations is

$$\left\langle\frac{1}{q_V^2}\right\rangle_a\equiv\frac{1}{2\pi}\int_0^{2\pi}\frac{{\rm d}\theta}{q_V^2(a,\theta)}=\frac{2+\nu^2}{2q_*^2}. \tag{3.6}$$

This expression is useful to evaluate the kink-mode drive for instabilities in § 7.

4. Frieman–Rotenberg formulation

For the linear stability analysis we employ the well known formulation by Frieman & Rotenberg (1960). In this formulation, perturbed quantities are expressed as functions of

https://doi.org/10.1017/S0022377820001178 Published online by Cambridge University Press

the quasi-Lagrangian plasma displacement ($\boldsymbol{\xi}$). For normal modes of the form

$$\boldsymbol{\xi}(\boldsymbol{r}, t) = \hat{\boldsymbol{\xi}}(R, Z)\exp(-\mathrm{i}(\omega t + n\varphi)), \tag{4.1}$$

the spectral equation for axisymmetric systems, in the case of plasmas with toroidal rotation only, reduces to

$$\tilde{\boldsymbol{F}}(\hat{\boldsymbol{\xi}}) = -\rho\bar{\omega}^2\hat{\boldsymbol{\xi}} - 2\mathrm{i}\rho\bar{\omega}\Omega\hat{\boldsymbol{e}}_Z \times \hat{\boldsymbol{\xi}} + (2\rho R\Omega\hat{\boldsymbol{\xi}}\cdot\boldsymbol{\nabla}\Omega)\hat{\boldsymbol{e}}_R - \tilde{\rho}\Omega^2 R\hat{\boldsymbol{e}}_R, \tag{4.2}$$

where the Doppler-shifted frequency is given by

$$\bar{\omega} \equiv \bar{\omega}(R, Z) = \omega + n\Omega(R, Z). \tag{4.3}$$

Hereafter, the 'hats' will be dropped; it should be understood that all perturbed quantities, and in particular the displacement vector, are time-independent. Utilizing the axisymmetric condition, it is possible to express the force operator as

$$\tilde{\boldsymbol{F}}(\boldsymbol{\xi}) = \frac{1}{\mu_o}\left\{\tilde{\boldsymbol{B}}_p\cdot\boldsymbol{\nabla}\boldsymbol{B} + \boldsymbol{B}\cdot\boldsymbol{\nabla}\tilde{\boldsymbol{B}}_p - \frac{2B_\varphi\tilde{B}_\varphi}{R}\hat{\boldsymbol{e}}_R + \left[\frac{B_R\tilde{B}_\varphi}{R} + \boldsymbol{B}\cdot\boldsymbol{\nabla}\tilde{B}_\varphi\right]\hat{\boldsymbol{e}}_\varphi\right\} - \boldsymbol{\nabla}\tilde{\Pi}. \tag{4.4}$$

This form of the force operator facilitates the computation of the plasma–vacuum boundary condition in § 7. The perturbed magnetic field has been decomposed into its poloidal and toroidal components,

$$\tilde{\boldsymbol{B}} = \tilde{\boldsymbol{B}}_p + \tilde{\boldsymbol{B}}_\varphi, \tag{4.5}$$

the remaining perturbed quantities are

$$\tilde{p} = -\gamma p\boldsymbol{\nabla}\cdot\boldsymbol{\xi} - \boldsymbol{\xi}\cdot\boldsymbol{\nabla}p, \tag{4.6}$$

$$\tilde{\rho} = -\boldsymbol{\nabla}\cdot(\rho\boldsymbol{\xi}) = -\rho\boldsymbol{\nabla}\cdot\boldsymbol{\xi} - \boldsymbol{\xi}\cdot\boldsymbol{\nabla}\rho, \tag{4.7}$$

$$\tilde{\boldsymbol{B}} = \boldsymbol{\nabla}\times(\boldsymbol{\xi}\times\boldsymbol{B}), \tag{4.8}$$

where the total pressure is given by the sum of the kinetic and magnetic contributions,

$$\tilde{\Pi} \equiv \tilde{p} + \frac{B\tilde{B}_\parallel}{\mu_o}, \tag{4.9}$$

here, $\parallel$ stands for a component parallel to the equilibrium magnetic field.

5. The Shear–Alfvén Law

The Shear–Alfvén law is obtained from the axisymmetric form of the momentum equation. This can be accomplished by either taking $\hat{\boldsymbol{e}}_\varphi\cdot\boldsymbol{\nabla}\times$ (4.2) and, subsequently, eliminating the $\partial_Z(B_\varphi\tilde{B}_\varphi)$ term from the Z component of the momentum equation, as done by Betti (1998) or, equivalently, by taking $\boldsymbol{\nabla}\varphi\cdot\boldsymbol{\nabla}\times[R^2$ (4.2)]. Loosely speaking, the resultant equation ($\mathcal{M} = \mathcal{L}$) consists of a 'magnetic part' ($\mathcal{M}$), which depends on the perturbed poloidal magnetic field; and of an 'inertial part' ($\mathcal{L}$), which depends on the

https://doi.org/10.1017/S0022377820001178 Published online by Cambridge University Press

perturbed density, velocity, and kinetic pressure. These contributions are

$$\mathcal{M} = -\nabla\varphi \cdot \nabla \times \left[R^2 \left[\tilde{\boldsymbol{B}}_p \times J_\varphi \hat{\boldsymbol{e}}_\varphi + \frac{\boldsymbol{B}}{\mu_o} \times (\nabla \times \tilde{\boldsymbol{B}}_p) \right] \right], \tag{5.1}$$

where J_φ is the equilibrium current density in the toroidal direction, and

$$\mathcal{L} = -\nabla \cdot (\rho\bar{\omega}^2 R\boldsymbol{\xi} \times \hat{\boldsymbol{e}}_\varphi) + \partial_Z [2\mathrm{i}\rho\bar{\omega}\Omega R\xi_\varphi + 2\rho R^2 \Omega \boldsymbol{\xi} \cdot \nabla\Omega - \tilde{\rho}\Omega^2 R^2 - 2\tilde{p}]. \tag{5.2}$$

One of the main differences between the stability analysis presented here and that developed in Betti (1998) for a configuration with a solid angular rotation profile, is that the flow shear drive $2\rho R^2 \Omega \boldsymbol{\xi} \cdot \nabla\Omega$ is absent in the latter model.

Even though the magnetic ($\mathcal{M}$) and inertial ($\mathcal{L}$) expressions are exact for axisymmetric configurations, equilibrium quantities are known to leading order in the inverse aspect ratio only. Accordingly, the stability analysis in this work can be accurate to leading order at most. The following stability analysis is based on the work by Betti (1998) for a configuration with rigid rotation.

6. Eigenvalue system of ODEs

The goal of this section is to obtain the m-th Fourier component of the Shear–Alfvén law. Perturbed quantities ($\tilde{f}$) are expressed as a superposition of poloidal modes in the usual way,

$$\tilde{f}(r, \varphi, \theta) = \sum_{m=-\infty}^{\infty} f_m(r) \exp(\mathrm{i}(m\theta - n\varphi)). \tag{6.1}$$

The calculation proceeds by introducing a stream function representation for the plasma displacement. The feasibility of this representation derives from the fact that the perturbed toroidal magnetic field is smaller than the poloidal one (in terms of the inverse aspect ratio). Following Waelbroeck (1996), we write $\boldsymbol{\xi} = \boldsymbol{\xi}^m + \xi_\parallel \hat{\boldsymbol{b}}$, where $\nabla\varphi \cdot \boldsymbol{\xi}^m = 0$. A straightforward manipulation shows that, for our equilibrium configuration, $\tilde{B}_\varphi \sim O(\epsilon^2 B_{\varphi o})$, and this leads (Waelbroeck 1996) to a stream function representation for the meridian plasma displacement component, $\boldsymbol{\xi}^m = F^{-1}R^2 \nabla U \times \nabla\varphi + O(\epsilon^2 a)$, where U is the stream function, as well as a potential representation for the perturbed magnetic field, $\tilde{\boldsymbol{B}} = \nabla\tilde{\Psi} \times \nabla\varphi + O(\epsilon^2 B_{\varphi o})$, where we have introduced a stream function for the perturbed poloidal magnetic flux as $\tilde{\Psi} \equiv F^{-1}R^2 \boldsymbol{B} \cdot \nabla U$.

The potential representation for the perturbed magnetic field is readily employed in the simplification of the magnetic contribution in the Shear–Alfvén law, yielding

$$\mathcal{M}_m = \left(\frac{\mathrm{i}B_{\varphi o}}{r\mu_o R_o} \right) \left\{ \left(-mh_m + \frac{1}{r}\frac{\mathrm{d}}{\mathrm{d}r}\left[r^3 \frac{\mathrm{d}\mu}{\mathrm{d}r} \right] \right) \frac{m\tilde{\Psi}_m}{r} + h_m \frac{\mathrm{d}}{\mathrm{d}r}\left[r\frac{\mathrm{d}\tilde{\Psi}_m}{\mathrm{d}r} \right] \right\} (1 + O(\nu)), \tag{6.2}$$

where

$$\mu(r) = 1/q(r) \tag{6.3}$$

and

$$h_m(r) = n - m\mu(r). \tag{6.4}$$

We have chosen to express $\mathcal{M}_m$ to leading order in ν. We recall that $\nu \sim O(1)$ by construction, but this quantity is always below unity, in accordance with the equilibrium

https://doi.org/10.1017/S0022377820001178 Published online by Cambridge University Press

β-limit (2.17). In this work, ν is regarded as an expansion parameter. In recognition of the non-circular nature of magnetic flux surfaces in high-β configurations (characterized here by ν), other works (Ito & Nakajima (2019), and references therein) have constructed magnetic flux coordinates in the presence of flows as the basis for stability analysis.

The computation continues by imposing incompressibility as follows:

$$\nabla \cdot \boldsymbol{\xi} = 0. \tag{6.5}$$

An *a posteriori* justification for this assumption has been provided by (Betti 1998, appendix C) in the context of a rigid rotating scenario. The validity condition for (6.5) turns out to be $\bar{\omega}^2/\omega_s^2 \ll 1$ where $\omega_s = V_s/R_o$ is the sound frequency (here, $V_s = \sqrt{\gamma p_o/\rho_o}$ is the sound speed). In the present work, $\Omega^2/\omega_s^2 \sim O(\epsilon) \ll 1$ by construction. Likewise, the growth rates of the resistive and ideal modes under consideration satisfy the validity condition (see § 9). In related work, the implications of the incompressibility constraint on the stability of the $m = n = 1$ internal kink mode have been extensively analysed by Wahlberg & Bondeson (1997). An *a posteriori* justification of (6.5) might be invoked for the present work as well. The incompressibility condition leads to a simple relation between the m-th Fourier component for the perturbed poloidal flux ($\tilde{\Psi}_m$), and for the radial plasma displacement (ξ_m),

$$\tilde{\Psi}_m = B_{\varphi o}\frac{r h_m \xi_m}{m}\left(1 + O(\nu)\right). \tag{6.6}$$

We now turn to the inertial term, given by (5.2). It is observed that the perturbed plasma density ($\tilde{\rho}$) is zero to leading order in the inverse aspect ratio. This follows from the fact that the leading-order density is constant (2.24), and the incompressibility condition. A beneficial consequence of the equilibrium model under consideration is that, as long as $\nu \gg \epsilon$, the Doppler, the Coriolis and the centrifugal contributions that appear in the Shear–Alfvén law, are one order (in ϵ) smaller than flow shear effects and may be neglected. Under this assumption, a straightforward algebraic manipulation leads to the m-th Fourier component of the inertial term,

$$\begin{aligned}\mathcal{L}_m = \left(\frac{-R_o\rho_o}{imr}\right)\Bigg\{&\frac{1}{r}\frac{\mathrm{d}}{\mathrm{d}r}\left[\left(\omega^2 r^3 - Kar^2\right)\frac{\mathrm{d}\xi_m}{\mathrm{d}r}\right]\\ &-\left[(m^2-1)\left(\omega^2 - a\frac{\mathrm{d}K}{\mathrm{d}r}\right)\right]\xi_m\Bigg\}\left(1+O(\epsilon)\right)\\ &-\mathrm{i}\left\{\frac{\left[(m-1)\tilde{p}_{m-1} + (m+1)\tilde{p}_{m+1}\right]}{r} + \left[\frac{\mathrm{d}\tilde{p}_{m+1}}{\mathrm{d}r} - \frac{\mathrm{d}\tilde{p}_{m-1}}{\mathrm{d}r}\right]\right\}.\end{aligned} \tag{6.7}$$

We have introduced the function

$$K(r) \equiv \frac{\nu\Omega_o^2}{\epsilon}\frac{\Psi_0(r)\Psi_1(r)}{a^4 B_{\varphi o}^2}. \tag{6.8}$$

It is recalled that $\Psi_0(r) \sim \Psi_1(r) \sim O(a^2 B_{\varphi o})$ are the contributions of the equilibrium poloidal flux in (2.13); it follows that $K(r) \sim O(\nu\Omega_o^2/\epsilon) \sim O(\nu\epsilon\omega_A^2)$. Here, $K(r)$ captures the flow shear drive for instabilities. Interestingly, this is a high-β toroidal effect, which disappears in the cylindrical limit ($\nu \to 0$).

Direct inspection of the linearized projection of the momentum equation along the magnetic field inform us that the flow-dependent terms in it are smaller than the flow

https://doi.org/10.1017/S0022377820001178 Published online by Cambridge University Press

shear drive in (6.7) (the K-term) by a factor $\sim\epsilon/\nu \ll 1$; hence, the former contributions are neglected. This results in a simple expression for the side bands of the perturbed pressure ($\tilde{p}_{m\pm1}$) as a function of the parallel plasma displacement which is substituted back into (6.7).

In writing down the m-th Fourier component of the inertial term ($\mathcal{L}_m$), we have neglected poloidal modes other than the principal. It is interesting to point out that while pressure gradient mode coupling is not captured across the plasma column in the stability analysis of Betti (1998) due to the features of the equilibrium considered there, here, it enters as an effect of order $\sim O(\nu f(\lambda)/q_*)$, where $f(\lambda) \sim O(1)$ has been defined in (2.22). Comparing the pressure gradient mode coupling ordering with the flow shear contribution (6.8) reveals that the former is dominant by a factor of ϵ. This is so because $\Omega/\omega_A \sim O(\epsilon)$ by construction. However, in order to make analytical progress, pressure gradient mode coupling across the plasma column is neglected in our work. In contrast, the eigenmode equation derived in Chapman *et al.* (2011) and Wahlberg *et al.* (2013), for low-β plasmas with $\Omega/\omega_A \sim O(\epsilon)$, retains equilibrium pressure gradient effects. In Betti (1998), harmonic coupling at the ODE level corresponds to small corrections of order $\sim O(\bar{\omega}^2/\omega_A^2)$ and is disregarded. In addition to implementing this approximation in our work, we also neglect mode coupling induced by the diffuse nature of the angular toroidal frequency. The interaction between different poloidal modes, which is characterized by ν, is retained at the plasma–vacuum transition only.

We are finally in a position to construct the m-th governing eigenmode ODE. Following Betti (1998) we introduce the functions

$$Y_m^2(r) \equiv r\frac{\mathrm{d}}{\mathrm{d}r}\left[\frac{(m-1)\omega^2}{h_{m+1}^2}\right] - r\frac{\mathrm{d}}{\mathrm{d}r}\left[\frac{(m+1)\omega^2}{h_{m-1}^2}\right] \tag{6.9}$$

and

$$\Gamma_m^2(r) \equiv \omega^2\left(1 + \frac{1}{h_{m+1}^2} + \frac{1}{h_{m-1}^2}\right). \tag{6.10}$$

Equations (6.9) and (6.10) differ from (31) and (32) of Betti (1998) in that the former pair does not capture centrifugal and Coriolis effects but the latter pair does. By equating the inertial term, from (6.7), with the magnetic term, from (6.2), we obtain

$$\begin{aligned}&\frac{1}{r}\frac{\mathrm{d}}{\mathrm{d}r}\left[([\Gamma_m^2 - \omega_A^2 h_m^2]r^3 - ar^2K)\frac{\mathrm{d}\xi_m}{\mathrm{d}r}\right]\\ &\quad - \left[(m^2-1)\left(\Gamma_m^2 - \omega_A^2 h_m^2 - a\frac{\mathrm{d}K}{\mathrm{d}r}\right) + Y_m^2\right]\xi_m = 0.\end{aligned} \tag{6.11}$$

Equation (6.11) should be compared with (38) of Betti (1998). It is observed that in the vanishing flow limit these equations formally agree. However, since profiles for the safety factor differ between the models, so do the $h_m(r)$ contributions in the eigenmode equations. In Betti (1998), there are two regions of interest: a central region with a constant safety factor and a thin region near the edge with a quadratic safety factor. Our model encompasses both possibilities: a constant safety factor is obtained when there is no magnetic shear ($\lambda = 0$) and a quadratic safety factor in the neighbourhood of the plasma edge is obtained by setting $\lambda = 5.78319$. Besides the eigenmode equation (6.11), the eigenvalue problem requires the specification of appropriate boundary conditions. They are supplied in the next section.

https://doi.org/10.1017/S0022377820001178 Published online by Cambridge University Press

7. Boundary conditions and wall effects

Boundary conditions are imposed at the plasma–vacuum interface, and at the outer material wall. Since the vacuum magnetic field is expressible as the gradient of a scalar potential ($\tilde{\boldsymbol{B}}_V = \boldsymbol{\nabla}\tilde{V}$), the condition for the continuity of the perturbed total pressure at the plasma–vacuum interface may be written as

$$\tilde{\Pi}_m(a) - \left[\!\left[\xi_r \frac{\partial}{\partial r}\left(p + \frac{B^2}{2\mu_o}\right)\right]\!\right]_m\Big|_a = \left[\frac{\boldsymbol{B}_V \cdot \boldsymbol{\nabla}\tilde{V}}{\mu_o}\right]_m\Big|_a . \tag{7.1}$$

Here, $[\![\ .\ ]\!]_m|_a$ represents the m-th Fourier component of the jump of a given quantity at the plasma edge. After a standard algebraic manipulation (see appendix B) it is possible to recast the boundary condition (7.1) in a way that explicitly depends on the Fourier components of the radial plasma displacement. In the final formulation, (B 9), Fourier components of the radial plasma displacement are coupled together by means of the ν coefficient, as defined in (2.14). Equation (B 9) incorporates the wall position (r_w) and wall resistive time ($\tau_w = \mu_o\, \mathrm{d}r_w/\eta_w$) through the function $\hat{\sigma}_l = \hat{\sigma}_l(\omega, \tau, r_w)$, as defined by (B 7).

Stability boundaries for cylindrical plasmas with no walls can be recovered from the eigenmode equation (6.11) and boundary conditions (B 9). This is accomplished by taking the vanishing ν limit, neglecting the $h_{m\pm1}$ coupling terms, and setting $\hat{\sigma}_l = 1$. In this limit, the model under consideration reduces to the pressureless configuration with a flat current profile and a jump at the plasma edge, which has been thoroughly studied in the context of the straight-tokamak approximation by means of the energy principle (Freidberg 2014). For that model, it is concluded that the condition for instability is

$$m - 1 < nq_a < m. \tag{7.2}$$

8. Solution technique: matrix-generated dispersion relation and multidimensional shooting method

For a collection of side bands $M_{\min} \le m \le M_{\max}$ ($m \neq 0$), the eigenvalue problem consists in solving $M_{\max} - M_{\min} + 1$ eigenmode ODEs (6.11), and determining the corresponding eigenfrequency ω, so that the set of coupling boundary conditions (B 9) is satisfied.

Harmonic contributions for the plasma displacement are required to be regular at $r = 0$. In this respect, it is observed that the governing ODE possesses a regular singularity at the origin, a situation which is typical. Ordinarily, the removal of the singularity is accomplished by expanding the coefficients of (6.11) as a power series centred at $r = 0$. An illustration of this procedure can be seen, for example, in Hazeltine & Meiss (2003). However, for the present model, there is a caveat: the closed-form analytic expression for Ψ_1 (A 5), introduced by López & Guazzotto (2017), which enters into the picture through the flow shear contribution (6.8) is undefined at $r = 0$, specifically,

$$\lim_{r\to 0} \Psi_1(r) = 0, \quad \text{but } \Psi_1(0) = \infty. \tag{8.1}$$

In order to deal with this unphysical limitation a new representation of Ψ_1, one that is $\mathcal{C}^\infty$ across the whole plasma column (including $r = 0$), is constructed in appendix A (A 6). Once the Ψ_1 part in the flow shear contribution is understood to be expressed in terms of (A 6), it is straightforward to reduce (6.11) into an equidimensional ODE in the

https://doi.org/10.1017/S0022377820001178 Published online by Cambridge University Press

neighbourhood of $r = 0$, and prove that the behaviour for the plasma displacement around the origin is the expected one,

$$\xi_m = c_m r^{-1+|m|}, \tag{8.2}$$

where, c_m are arbitrary complex constants.

Given a set of c_m, one of these constants can be chosen in an arbitrary way without loss of generality (say, the one corresponding to $m = M_{\max}$). Thus, the eigenvalue problem consists of determining $M_{\max} - M_{\min} + 1$ complex numbers: $\{\omega, c_{M_{\min}}, c_{M_{\min}+1}, \ldots, c_{M_{\max}-1}\}$ consistent with boundary conditions. In regards to the numerical integration, it is carried out starting at a point r_o (with $0 < r_o \ll a$) where continuity of the plasma displacement and its derivative, as computed from (8.2), are imposed. Since the closed-form analytical expression for Ψ_1 (A 5) is regular in the interval $[r_o, a]$, it is the one employed for numerical integration. In this way, the stability eigenvalue problem has been recast as a multidimensional shooting method.

In a multidimensional shooting method, good initial guesses are critical in order to achieve convergence. It is fortunate that a robust method to compute such initial guesses can be developed for the problem at hand. Despite the fact that the governing ODE must be solved numerically (in general), static plasmas with no magnetic shear admit a solution identical to (8.2), not only at the origin's neighbourhood but across the whole plasma column. In this regime, the set of boundary conditions reduces to a linear system for the mode amplitudes (c_m), and its determinant leads to the system's dispersion relation, which is solvable by a root-finding method over the complex plane. Therefore, in this regime, the complete set of eigenvalue/eigenvectors pairs is computable with no uncertainty (up to numerical errors); they constitute excellent initial guesses. Then, by progressively changing equilibrium parameters, it is possible to explore regions of parameter space with finite values for the velocity and the magnetic shear.

9. The stability of $n = 1$ modes surrounded by ideal and resistive walls

Stability boundaries for static plasmas with no magnetic shear surrounded by an ideal wall are shown in figure 2. Plasmas with vanishing magnetic shear admit a simple equilibrium solution,

$$\lim_{\langle s\rangle \to 0} \Psi(r, \theta) = \frac{1}{2q_* a^2}[(r^2 - a^2) + \nu(r^3 - ra^2)\cos(\theta)], \tag{9.1}$$

which corresponds to the high-β static model developed by Freidberg (2014, equation (6.103)). The computation of figure 2 utilizes (9.1) for the equilibrium solution instead of the general equations (A 4) and (A 5), which are valid for an arbitrary value of the magnetic shear. Stability curves are found by fixing the kink-safety factor and plasma pressure (ν), progressively increasing the wall radius and computing, at each (ν, r_w) point, the complete set of eigenvector/eigenvalue pairs by solving the matrix-generated dispersion relation. Marginal stability is reached when the growth rate of the fastest-growing mode vanishes ($\omega_I \equiv \mathrm{Im}\{\omega\} = 0$). Stability boundaries are found for the $n = 1$ toroidal mode by considering a narrow poloidal spectrum of only five modes, $m = 1, 2, 3, 4, 5$. In contrast, the stability of highly shaped configurations has been studied in the past by retaining the coupling of up to 45 poloidal modes (Rhodes *et al.* 2018).

The condition for instability (7.2) indicates that for $n = 1$ the plasma is unstable in the entire range $0 \leq q_a \leq \infty$. As illustrated in figure 2, for the stabilization of this ideal-plasma external kink mode (IPKM) it is necessary to bring the wall from infinity to a finite position near the plasma. Our study focuses on external kink modes when there

https://doi.org/10.1017/S0022377820001178 Published online by Cambridge University Press

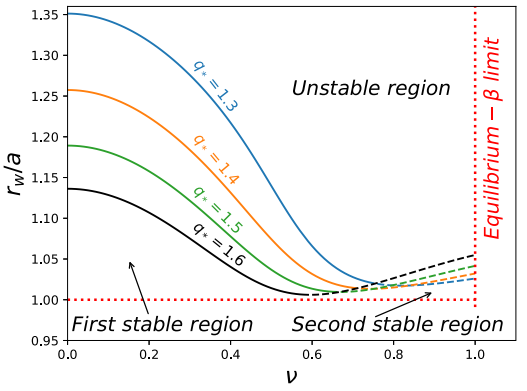


FIGURE 2. Marginal stability boundaries against $n = 1$ external kink modes for a static plasma with zero magnetic shear, an ideal wall and varying values of the kink-safety factor. The $r_w/a = 1$ horizontal line corresponds to the situation in which the wall is positioned at the plasma edge. In the $\langle s \rangle = 0$, $\langle \Omega \rangle = 0$ configuration considered here, the diffuse model simplifies to the high-β model of Freidberg (2014).

are no resonant surfaces located inside the plasma. In principle, to avoid the onset of the $m/n = 2/1$ tearing mode an upper limit $q_a < 2$ should be imposed, which (according to (2.16)) would translate into an upper bound for ν. However, despite the fact that toroidal effects are considered in the stability analysis, resonances enter as if the configuration was cylindrical (see (2.19), (6.3) and (6.4)) and this ν-dependent upper limit is not captured by the stability model. In any case, in order to keep track of this approximation, the dashed part of the marginal stability curves in figure 2 indicate that these critical values for ν have been surpassed. Stability curves are computed up to the equilibrium β-limit $\nu < 1$ (2.17).

As in other stability analyses (Betti 1998; Rhodes *et al.* 2018), a second region of stability is found in the high-β regime for the present model. Among the possibilities shown in figure 2, it would be desirable to operate at $q_* = 1.6$, since this option offers more 'high-β room' than the others ($q_* = 1.3, 1.4, 1.5$). At a fixed wall radius, accessing a high-β regime is accomplished by transiting across a region of unstable β. Hypothetically, this transition could be aided with the addition of magnetic shear ($\langle s \rangle$). It is recalled that the equilibrium solution under consideration is able to accommodate changing values for the mean magnetic shear, as explained through (2.18)–(2.23) and shown in figures 1(*a*) and 1(*b*). Figure 3(*b*) illustrates the suppression of the fastest-growing mode as the average magnetic shear is increased at varying distances above ($\Delta r_w/a$) the marginal stability wall position when it is closest to the plasma edge ($r_w/a = 1.007$); a situation which occurs when the coupling parameter is $\nu = 0.596$ (as can be seen from figure 2). Starting at $r_w/a = 1.007$ and $\langle s \rangle = 0$, we move upward into the unstable regime a distance $\Delta r_w/a$, this results in the onset of finite growing IPKMs; however, a subsequent application of a positive magnetic shear is able to completely suppress the instabilities. Unfortunately, despite the fact that the addition of magnetic shear raises the stability boundaries, this effect is small at the global minimum of the $q_* = 1.6$ curve. Indeed, for a mean magnetic shear of $\langle s \rangle \sim 0.4$, the stability boundary would move up around $\Delta r_w = 0.39$ cm in a plasma with a minor radius of one metre. In contrast, at zero β, the same strength for the magnetic shear raises the stability boundary approximately $\Delta r_w = 4.93$ cm (see figure 3*a*). This indicates that magnetic shear stabilization is more effective in the low-β regime. For the $q_* = 1.6$ case, increasing the value of the magnetic shear above $\langle s \rangle = 0.48$ results in

https://doi.org/10.1017/S0022377820001178 Published online by Cambridge University Press

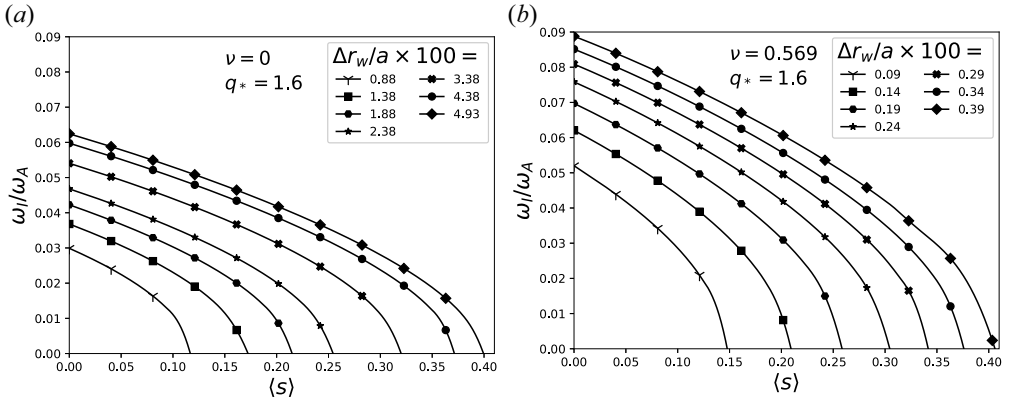


FIGURE 3. Magnetic shear stabilization of the $n = 1$ mode for a plasma surrounded by an ideal wall and with $q_* = 1.6$ at (a) zero pressure ($\nu = 0$) and (b) finite pressure ($\nu = 0.596$). In the vanishing magnetic shear scenario ($\langle s \rangle = 0$), figure 2 indicates that the marginal wall position for case (a) is $r_w/a = 1.136$, while that for case (b) is $r_w/a = 1.007$. Starting at those positions, we travel a distance $\Delta r_w/a$ upwards into the unstable regime without increasing the magnetic shear; this results in finite growth rates (ω_I/ω_A). At those fixed locations, a subsequent increase in the magnetic shear leads to the stabilization of the plasma column.

internal resonances; it is the purpose of future work to determine the effect of magnetic shear in those circumstances.

The consequence of adding a finite mild flow shear drive in the presence of ideal and resistive walls is exemplified in figure 4 for equilibria with angular frequencies ($\langle \Omega \rangle$) of a considerable fraction of the Alfvén frequency. Here, $\langle \Omega \rangle$ is defined as an average over the plasma volume,

$$\langle \Omega \rangle = \frac{1}{V_p} \int \Omega(\Psi)\, \mathrm{d}^3 r = -\frac{\Omega_o\, {}_0\tilde{F}_1\left(;3;-\dfrac{\lambda}{4}\right)}{2q_*\, {}_0\tilde{F}_1\left(;2;-\dfrac{\lambda}{4}\right)}, \tag{9.2}$$

where λ is, in turn, given by (2.23). For a fixed wall radius of $r_w/a = 1.05$ and a kink-safety factor of $q_* = 1.6$, figure 4(a) illustrates the onset of IPKMs as the pressure increases and the subsequent transition into the second stability region. Meanwhile, figure 4(b) exemplifies the onset of ideal-plasma resistive wall modes (IPRWMs). It is well understood that IPRWMs eliminate the stabilizing influence of the wall on times comparable to the diffusion time, which we have chosen as $\tau_w\omega_A = 2 \times 10^3$ and $\tau_w\omega_A = 2 \times 10^4$. The IPRWMs corresponding to static plasmas in figure 4(b) are in qualitative agreement with figure 5 of Betti (1998), which employs $\tau_w\omega_A = 2 \times 10^4$, and with figures 2 and 3 of Rhodes *et al.* (2018), where $\tau_w\omega_A = 10^3$. It has been pointed out that at zero β the model under consideration is unstable if the wall is at infinity (7.2), accordingly, figure 4(b) shows residual IPRWMs at zero β. On the contrary, the models considered by Betti (1998) and by Rhodes *et al.* (2018) are stable below critical β values, and it is the purpose of those articles to determine the degree to which rigid rotation can increase these β-limits. In the absence of rotation, resistive wall tearing modes constitute the least stable modes, consequently, plasma resistivity should be taken into account (Betti 1998; Rhodes *et al.* 2018). Presently, our work considers ideal plasmas only, it is the aim of future work to incorporate plasma resistivity.

https://doi.org/10.1017/S0022377820001178 Published online by Cambridge University Press

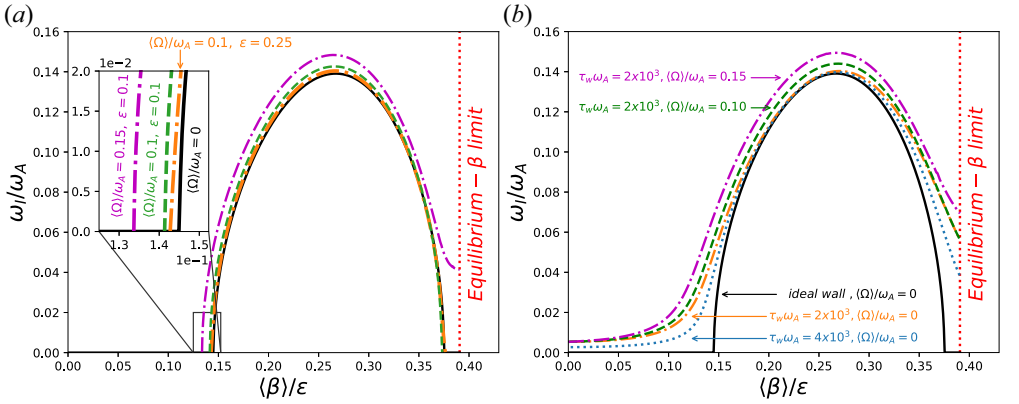


FIGURE 4. Comparison of growth rates of the $n = 1$ mode for plasmas with diffuse toroidal rotation in the presence of (*a*) ideal walls and (*b*) resistive walls. The comparison is performed at varying rotating frequencies of a significant fraction of the Alfvén frequency. Here, $\langle\Omega(\Psi)\rangle$ represents the average toroidal rotation over the plasma volume. In all cases $q_* = 1.6$, $\langle s\rangle = 0$ and $r_w/a = 1.05$. In panel (*b*) $\epsilon = 0.1$.

The combined effect of resistivity and flow shear results in a magnification of the growth rates for all β (see figure 4*b*). Figure 4(*a*) illustrates that IPKMs growth rates increase with rotation, and that β-limits decrease with it. It is recalled that in the present stability analysis flow shear dominates over all other velocity dependent contributions as long as $\nu \gg \epsilon$. In figure 4(*a*), this assumption is better satisfied for the $\epsilon = 0.1$ case than for the more realistic $\epsilon = 0.25$ scenario; however, it is beneficial to be able to visualize the effect of flow shear alone, even if that is possible in this small ϵ-limit only. When ν and ϵ are comparable, centrifugal and Coriolis contributions should be retained.

In order to compare the effect of flow for the diffuse scenario with a rigid rotation configuration, the model developed by Betti (1998) is reconsidered. In the sharp-boundary formalism with a rigid angular toroidal frequency introduced by Betti (1998), the plasma column is composed of an inner region with a constant safety factor ('the current channel') and a thin outer region where the safety factor grows quadratically ('the plasma edge'). Due to the fact that our model is able to accommodate a flat safety factor ($\langle s\rangle = 0$) we opt for discarding the plasma edge from the sharp-boundary model. The removal of the plasma edge is accomplished by a straightforward modification of the boundary conditions given by equation (67) from Betti (1998). In the vanishing flow limit, the remaining differences between the sharp boundary and diffuse models are due to high-β terms in the boundary conditions: the ballooning and the kink mode drives differ, and the μ_1 toroidal contribution (B 2) is unique to the diffuse model in this work. For static plasmas, figure 5 illustrates marginal stability curves for both scenarios. As predicted, the models agree in the vanishing β-limit but strongly differ at higher β.

A meaningful comparison of the effect of flow between the diffuse and sharp-boundary models should be performed in the low-β regime, yet, the flow shear drive for instabilities is a high-β toroidal effect that vanishes in the cylindrical limit (6.8). Thus, we are led to compare the effect of flow in situations where static scenarios significantly differ. The comparison is performed at $\nu = 0.4$, for a plasma with $\epsilon = 0.1$ (so that the validity condition $\nu \gg \epsilon$ is satisfied) and kink-safety factors of $q_* = 1.3$ and $q_* = 1.6$. Let us consider the marginal stability curve corresponding to a kink-safety factor of $q_* = 1.6$ first. As seen in figure 5, the wall position for marginal stability (at $\nu = 0.4$) is $r_w/a = 1.040$ in

https://doi.org/10.1017/S0022377820001178 Published online by Cambridge University Press

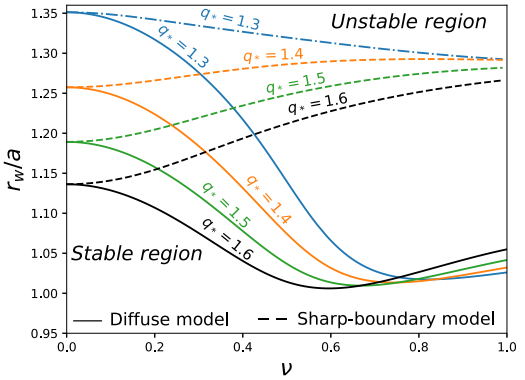


FIGURE 5. Marginal stability boundaries against $n = 1$ external kink modes for static plasmas with ideal walls and varying values of the kink-safety factor. The solid curves correspond to our model in the case of a constant safety factor ($\langle s \rangle = 0$ and $q_* = q_a$), these stability curves are the same as in figure 2, but are replotted here to ease their comparison with the sharp-boundary model. The dashed lines correspond to the sharp-boundary model introduced in Betti (1998) but with a constant safety factor across the whole plasma column, i.e. the so-called 'plasma edge': a region where the safety factor grows quadratically, has been self-consistently removed from that model. In the latter model, $\langle q_V \rangle_a$ is an independent variable. Here, it has been chosen as $\langle q_V \rangle_a = q_a$ in order to mimic (3.5), which is valid for the diffuse model.

the case of the diffuse model, and $r_w/a = 1.194$ for the sharp boundary one. A variation in the rotation frequency results in a modification of the wall position for marginal stability. Here, $\Delta r_w/a$ measures this variation with respect to the wall position for marginal stability in the absence of flow. Figure 6(a) shows the results of these calculations for several rotation frequencies at a significant fraction of the Alfvén frequency. This figure illustrates that in order to suppress the external kink modes driven by flow shear it is necessary to displace the wall towards the plasma edge. The opposite behaviour is experienced in the case with rigid rotation. Nevertheless, for plasmas with the same average kinetic energy, the $\Delta r_w/a$ modifications in the rigid rotation model are significantly larger than those in the diffuse scenario. This difference is (partly) attributed to the fact that in the sharp-boundary model, rotation produces an enhancement on the value of β that enters in the boundary conditions. Essentially, the form for the equilibrium pressure profile $p(R) = p_o \exp[(R^2/R_o^2 - 1)M^2/2]$, is responsible for β-enhancement by a $(1 + M^2/2)$ factor. In contrast, $\Omega(\Psi)$ and $p(\Psi)$ are not as tightly coupled in the diffuse model (although the constraints given by (2.20), (2.21), (2.27) and (2.28) should be satisfied). In order to accentuate the destabilizing effect of flow shear, which scales as $\sim 1/q_*^2$ ((2.13), (6.8), (A 4) and (A 5)), we consider a configuration with a lower value for the kink-safety factor next: $q_* = 1.3$. Starting at $\nu = 0.4$, and travelling along the $q_* = 1.3$ curve for the sharp-boundary model, an increase in β pushes the wall position r_w/a towards the plasma (figure 5). Accordingly, figure 6(b) illustrates the destabilizing influence of rigid rotation for $\Omega/\omega_A = 0.075$ and $\Omega/\omega_A = 0.1$. At even higher rotation values ($\Omega/\omega_A = 0.15$), rigid flow is stabilizing. Contrary to figure 6(a), in figure 6(b) it is observed that the $\Delta r_w/a$ modifications due to flow shear are of comparable order, and in fact larger, than those produced when the plasma rotates as a solid body.

The comparison of the IPKM growth rates for plasmas with diffuse and rigid angular toroidal rotations in figure 6 are only qualitative. The stability of configurations where it is possible to control the level of flow shear, and where toroidal effects are retained, are

https://doi.org/10.1017/S0022377820001178 Published online by Cambridge University Press

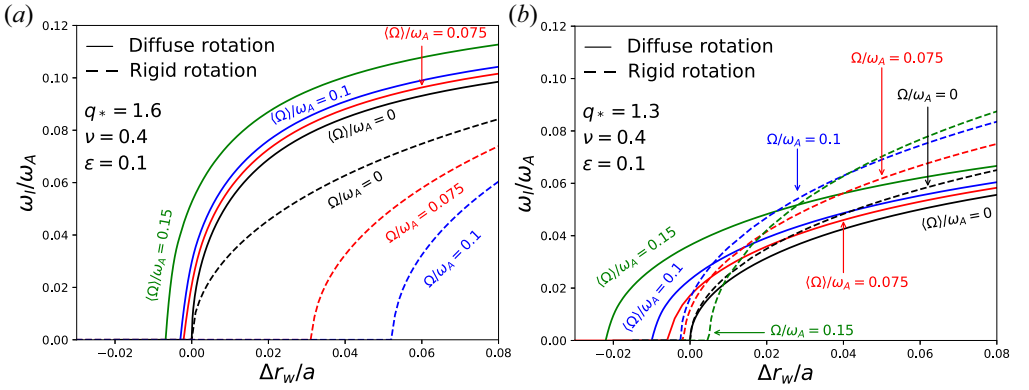


FIGURE 6. Comparison of growth rates of the $n = 1$ mode for plasmas with diffuse and rigid angular toroidal rotations. The comparison is performed at varying rotating frequencies of a significant fraction of the Alfvén frequency. Here, $\langle\Omega(\Psi)\rangle$ represents the average toroidal rotation over the plasma volume. Walls are assumed to be ideal, $\nu = 0.4$, $\epsilon = 0.1$ and the kink-safety factor is equal to (*a*) $q_* = 1.6$ and (*b*) $q_* = 1.3$. Here, $\Delta r_w/a$ represents the displacement of the wall position for marginal stability in the presence of flow with respect to its position in the absence of it. Positions for marginal stability for static plasmas are given in figure 5. For case (*a*), $q_* = 1.6$, the positions of marginal stability for the diffuse and the rigid rotation scenario are $r_w/a = 1.040$ and $r_w/a = 1.194$, respectively. For case (*b*), $q_* = 1.3$, these positions are $r_w/a = 1.217$ and $r_w/a = 1.327$, in the same order. In panel (*b*), the $\Delta r_w/a$ modifications due to flow shear are larger than the ones due to rigid rotation; the opposite occurs in panel (*a*).

probably better suited to be studied employing full numerical implementations (Chapman *et al.* 2012), but at the expense of capturing centrifugal and Coriolis effects as well. In this work, we have evaluated the effect of a high-β flow shear drive while ordering out other velocity dependent contributions.

10. Summary and discussion

We have studied the linear stability of external $n = 1$ modes for a tokamak plasma with a diffuse toroidal velocity profile and positive average finite magnetic shear. The effects of ideal and resistive walls are also considered. We have illustrated the stabilizing influence of the magnetic shear and the destabilizing nature of a global flow shear drive.

The stability analysis has been built upon a closed-form analytical equilibrium for a circular cross-section that is accurate to leading order in the inverse aspect ratio. In consequence, this ordering has been inherited at the stability level. Poloidal coupling is disregarded across the plasma column but is retained at the plasma–vacuum transition. Resonances enter in the stability analysis as if the configuration were cylindrical. Internal resonances are out of the scope of the present work and are avoided by selecting appropriate equilibrium parameters. Toroidal effects do enter into the stability picture; most notably, the flow shear drive for instabilities (6.8) is a high-β toroidal effect. It has been determined that this effect is larger than centrifugal and Coriolis contributions provided that $\nu \gg \epsilon$. We perform a qualitative comparison of our model against a sharp-boundary scenario with a rigid angular toroidal frequency, which is based upon Betti (1998). Despite the fact that there are scenarios in which the destabilizing influence of flow shear is small as compared with the stability modifications in the presence of rigid rotation (figure 6*a*), figure 6(*b*) reveals that the (ideal) wall position for marginal

https://doi.org/10.1017/S0022377820001178 Published online by Cambridge University Press

stability might experience variations ($\Delta r_w/a$) of the same order of magnitude due to the destabilizing influence of a global flow shear drive, as in the case with rigid rotation.

The stability eigenvalue problem has been solved by implementing a multidimensional shooting method for the coupled poloidal harmonics. For static plasmas with no magnetic shear the eigenmode equation admits a trivial solution (8.2). This leads to a dispersion relation that is solvable with standard root finding methods. Eigenvalue/eigenvector pairs computed in this simple scenario function as robust initial guesses for the shooting method in situations with finite magnetic shear, toroidal velocity and resistive walls. The numerical implementation shoots from a position near the origin ($r = 0$) 'pointing towards' the plasma–vacuum transition. Unfortunately, due to the fact that the equilibrium introduced in López & Guazzotto (2017) possesses a singularity at the origin, the flow shear drive introduces this unphysical singularity at the eigenmode equation level. This issue has been addressed by constructing an alternative representation for the equilibrium that is regular on the complete plasma domain (appendix A).

Acknowledgements

This work has been supported by the US Department of Energy under Contract no. DE-FG02-93ER54215. This article was completed in part with resources provided by Auburn University COSAM IT and the Hopper Cluster.

Editor Paolo Ricci thanks the referees for their advice in evaluating this article.

Declaration of interests

The authors report no conflict of interest.

Appendix A. Singularity removal by means of a series-form solution for the equilibrium

It has been shown (López & Guazzotto 2017) that under the ordering assumptions discussed in § 2 the leading-order poloidal flux satisfies the inhomogeneous Helmholtz equation,

$$\left(\nabla^2 + \frac{\lambda}{a^2}\right)\Psi(r,\theta) = B_{\varphi o}\left[A + \frac{Cr}{a}\cos\theta\right], \tag{A 1}$$

with Dirichlet boundary conditions (2.12); here,

$$A = \frac{\sqrt{\lambda}J_0(\sqrt{\lambda})}{q_* J_1(\sqrt{\lambda})}, \quad C = \frac{4\nu J_1(\sqrt{\lambda})}{q_*\,{}_0\tilde{F}_1\left(;3;-\frac{\lambda}{4}\right)\sqrt{\lambda}}. \tag{A 2a,b}$$

It has been shown (López & Guazzotto 2017) that (A 1) has a solution of the form

$$\Psi(r,\theta) = \Psi_0(r) + \nu\Psi_1(r)\cos(\theta), \tag{A 3}$$

where

$$\frac{\Psi_0(r)}{a^2 B_{\varphi o}} = \frac{J_0(\sqrt{\lambda}) - J_0(\sqrt{\lambda}r/a)}{q_* J_1(\sqrt{\lambda})\sqrt{\lambda}} \tag{A 4}$$

https://doi.org/10.1017/S0022377820001178 Published online by Cambridge University Press

and

$$\frac{\Psi_1(r)}{a^2 B_{\varphi o}} = \frac{2J_1(\sqrt{\lambda})\pi}{q_{*\,0}\tilde{F}_1\left(;3;-\frac{\lambda}{4}\right)\lambda}\left\{\left(\frac{r}{a}\right)^2 J_2\left(\sqrt{\lambda}\frac{r}{a}\right) Y_1\left(\sqrt{\lambda}\frac{r}{a}\right)\right.$$
$$-J_1\left(\sqrt{\lambda}\frac{r}{a}\right)\left[\frac{J_2(\sqrt{\lambda})Y_1(\sqrt{\lambda})}{J_1(\sqrt{\lambda})} - G^{2,1}_{2,4}\left(\frac{\sqrt{\lambda}}{2},\frac{1}{2}\middle|\begin{matrix}0,-\frac{1}{2}\\ 0,1,-1,-\frac{1}{2}\end{matrix}\right)\right.$$
$$\left.\left.+\frac{\sqrt{\lambda}}{2}\left(\frac{r}{a}\right)^3 G^{2,1}_{2,4}\left(\frac{\sqrt{\lambda}}{2}\frac{r}{a},\frac{1}{2}\middle|\begin{matrix}-\frac{1}{2},-1\\ -\frac{1}{2},\frac{1}{2},-\frac{3}{2},-1\end{matrix}\right)\right]\right\}. \tag{A 5}$$

Here, $G^{2,1}_{2,4}$ represents the Meijer G-function (DLMF 2020, § 16.17).

The first step towards the implementation of the multidimensional shooting method is to solve the governing eigenmode equation (6.11) at the origin's neighbourhood ($r = 0$). It is observed that the flow shear drive introduces an unphysical singularity into the ODE when Ψ_1 is expressed in terms of (A 5). This is because the $G^{2,1}_{2,4}$ Meijer G-function and the first Bessel function of the second kind are singular at $r = 0$. To solve this issue, an alternative representation for Ψ_1 is constructed next.

It is possible to build a Green's function for (A 1) that involves an expansion in a complete set of functions in both the θ and r directions. This leads to the following series-form representation of Ψ_1:

$$\frac{\Psi_1(r)}{a^2 B_{\varphi o}} = \frac{32J_1(\sqrt{\lambda})}{q_*\sqrt{\lambda}\,{}_0\tilde{F}_1\left(;3;-\frac{\lambda}{4}\right)}\sum_{k=1}^{\infty}\frac{J_2(j_{1,k})J_1\left(rj_{1,k}/a\right)}{j_{1,k}(\lambda-(j_{1,k})^2)(J_0(j_{1,k})-J_2(j_{1,k}))^2}, \tag{A 6}$$

where $j_{1,k}$ is the k-th zero of the second Bessel function of the first kind. Contrary to (A 5), this representation for Ψ_1 is regular at $r = 0$.

Appendix B. Further details on the boundary conditions and wall effects

In this section, we adapt the discussion of Freidberg (2014) in order to reduce (7.1) into a set of useful boundary conditions.

An expression for the perturbed total pressure ($\tilde{\Pi}_m(a)$) originates from the poloidal component of the perturbed momentum equation. This expression, in turn, depends on side bands for the perturbed toroidal magnetic field ($\tilde{B}_{\varphi,m\pm1}$). The projection of the momentum equation into the toroidal direction results in an ODE for the side bands $\tilde{B}_{\varphi,m\pm1}$, fortunately, this ODE reduces to a simple algebraic expression to leading order in ν. Ultimately, it can be shown that $\tilde{\Pi}_m(a)$ depends on Ξ^2_m and μ_1, as defined by

$$\Xi^2_m = m\left[\omega^2\left(\frac{1}{h^2_{m-1}}-\frac{1}{h^2_{m+1}}\right)-\frac{a}{m}\frac{h'_m}{h_m}\Gamma^2_m\right]\Bigg|_a \tag{B 1}$$

and

$$\mu_1(r) = \frac{1}{rB_{\varphi o}}\frac{\mathrm{d}\Psi_1}{\mathrm{d}r}. \tag{B 2}$$

https://doi.org/10.1017/S0022377820001178 Published online by Cambridge University Press

Equation (B 1) differs from (62) in Betti (1998) in that the former does not capture centrifugal and Coriolis effects but the latter does. Additionally, (62) is valid when the safety factor is quadratic at the plasma edge, while (B 1) accepts an arbitrary safety factor. On the other hand, μ_1 is a new toroidal effect that originates from the angular dependence of the equilibrium poloidal flux (2.13).

From the equilibrium momentum equation, in combination with the average of the inverse square vacuum safety factor, we obtain

$$\left[\left[\xi_r \frac{\partial}{\partial r}\left(p + \frac{B^2}{2\mu_o}\right)\right]\right]_m\Big|_a = -\frac{3\nu^2 B_{\varphi o}^2 a}{2q_*^2 \mu_o R_o^2}\xi_m(a). \tag{B 3}$$

This expression is recognized as a kink-mode drive for instabilities. In surface current models from the literature (Goedbloed (1982); Betti (1998); Freidberg (2014), to cite a few) an additional, ballooning-mode drive, arises as a term proportional to the plasma pressure times the average curvature across the interface; however, this instability drive vanishes for the pressure model under consideration ((2.25) and (2.26*a*,*b*)).

Wall effects are incorporated by means of the vacuum magnetic field. To leading order in the inverse aspect ratio, the m-th Fourier component for the inner ($a < r < r_w$) and outer ($r_w < r$) vacuum magnetic potentials are easily computable (Freidberg 2007). These expressions, together with the continuity requirement for the normal component of the magnetic field, $[[\tilde{B}_r]]_a = 0$, and the jump conditions for the magnetic potentials under the thin wall approximation (Guazzotto, Freidberg & Betti 2008),

$$\left.\frac{\partial \tilde{V}_m^{\text{outer}}}{\partial r}\right|_{r_w} = \left.\frac{\partial \tilde{V}_m^{\text{inner}}}{\partial r}\right|_{r_w}, \tag{B 4}$$

$$\left.\frac{\partial^2 \tilde{V}_m^{\text{outer}}}{\partial r^2}\right|_{r_w} = \left.\frac{\partial^2 \tilde{V}_m^{\text{inner}}}{\partial r^2}\right|_{r_w} - \frac{\mathrm{i}\omega\mu_o d}{\eta_w}\left.\frac{\partial \tilde{V}_m^{\text{inner}}}{\partial r}\right|_{r_w}, \tag{B 5}$$

are utilized to determine the m-th ($m \neq 0$) component for the right-hand side of (7.1) in terms of the perturbed plasma displacement, wall location and resistive time. The poloidal component of the equilibrium vacuum field shown in (3.2) enters in this calculation, the end result is

$$\begin{aligned}\frac{R_o^2}{a}\left[\frac{\boldsymbol{B}_V\cdot\nabla\tilde{V}}{B_{\varphi o}^2}\right]_m\Big|_a = {}& \hat{\sigma}_{m-1}\frac{|m-1|\nu^2}{4q_*^2}\xi_{m-2} + \hat{\sigma}_{m+1}\frac{|m+1|\nu^2}{4q_*^2}\xi_{m+2} \\ & - \frac{\nu}{2q_*}\left[\hat{\sigma}_m \operatorname{sgn}(m) h_m + \hat{\sigma}_{m-1}\operatorname{sgn}(m-1)h_{m-1}\right]\xi_{m-1} \\ & - \frac{\nu}{2q_*}\left[\hat{\sigma}_m \operatorname{sgn}(m) h_m + \hat{\sigma}_{m+1}\operatorname{sgn}(m+1)h_{m+1}\right]\xi_{m+1} \\ & + \left[\hat{\sigma}_{m-1}\frac{|m-1|\nu^2}{4q_*^2} + \frac{\hat{\sigma}_m}{|m|}h_m^2 + \hat{\sigma}_{m+1}\frac{|m+1|\nu^2}{4q_*^2}\right]\xi_m.\end{aligned} \tag{B 6}$$

It should be pointed out that ξ_0 vanishes in view of the incompressibility condition (Freidberg & Haas 1973). In the above, sgn stands for the sign function. Here, $\hat{\sigma}_l$ is given

https://doi.org/10.1017/S0022377820001178 Published online by Cambridge University Press

by

$$\hat{\sigma}_l = \frac{2|l| - \mathrm{i}\omega\tau_w\left[1 + (a/r_w)^{2|l|}\right]}{2|l| - \mathrm{i}\omega\tau_w\left[1 - (a/r_w)^{2|l|}\right]}. \tag{B 7}$$

It is observed that the perfectly conducting wall scenario can be recovered in the $\tau_w \to \infty$ limit. In this case,

$$\hat{\sigma}_l = \frac{1 + (a/r_w)^{2|l|}}{1 - (a/r_w)^{2|l|}}. \tag{B 8}$$

In conclusion, the m-th ($m \neq 0$) plasma–vacuum matching condition, together with material wall effects, can be written as the following finite superposition of poloidal modes:

$$\begin{aligned}\frac{R_o^2}{B_{\varphi o}}\left[\boldsymbol{B}_V \cdot \boldsymbol{\nabla}\tilde{V}\right]_m\Big|_a &= \left[\frac{\Gamma_m^2}{\omega_A^2 h_m^2} - 1\right]\Big|_a \frac{h_m(a)}{m} a\tilde{\Psi}'_m(a) \\ &+ \frac{\Xi_m^2 \tilde{\Psi}_m(a)}{m\omega_A^2 h_m(a)} + \frac{3\nu^2 a B_{\varphi o}}{2q_*^2}\xi_m(a) - \left[a\mu'_0 + 2\mu_0\right]\tilde{\Psi}_m \\ &+ \frac{\nu}{2}\left[\mu_1 a\left[\tilde{\Psi}'_{m+1} + \tilde{\Psi}'_{m-1}\right] - \frac{a\mu'_1 + 2\mu_1}{m}\left[(m+1)\tilde{\Psi}_{m+1} + (m-1)\tilde{\Psi}_{m-1}\right]\right]\Big|_a, \end{aligned} \tag{B 9}$$

where the left-hand side is given by (B 6), and $\tilde{\Psi}_m$ should be understood to be expressed in terms of ξ_m in accordance to (6.6).

REFERENCES

Baylor, L. R., Burrell, K. H., Groebner, R. J., Houlberg, W. A., Ernst, D. P., Murakami, M. & Wade, M. R. 2004 Comparison of toroidal rotation velocities of different impurity ions in the DIII-D tokamak. *Phys. Plasmas* **11** (6), 3100–3105.

Betti, R. 1998 Beta limits for the $N = 1$ mode in rotating-toroidal-resistive plasmas surrounded by a resistive wall. *Phys. Plasmas* **5** (10), 3615–3631.

Betti, R. & Freidberg, J. P. 1995 Stability analysis of resistive wall kink modes in rotating plasmas. *Phys. Rev. Lett.* **74**, 2949–2952.

Bondeson, A. & Ward, D. J. 1994 Stabilization of external modes in tokamaks by resistive walls and plasma rotation. *Phys. Rev. Lett.* **72**, 2709–2712.

Brunetti, D., Lazzaro, E. & Nowak, S. 2017 Ideal and resistive magnetohydrodynamic instabilities in cylindrical geometry with a sheared flow along the axis. *Plasma Phys. Control. Fusion* **59** (5), 055012.

Catto, P. J., Bernstein, I. B. & Tessarotto, M. 1987 Ion transport in toroidally rotating tokamak plasmas. *Phys. Fluids* **30** (9), 2784–2795.

Chandrasekhar, S. 1961 *Hydrodynamic and Hydromagnetic Stability*. Clarendon Press.

Chapman, I. T., Brown, S., Kemp, R. & Walkden, N. R. 2012 Toroidal velocity shear Kelvin–Helmholtz instabilities in strongly rotating tokamak plasmas. *Nucl. Fusion* **52** (4), 042005.

Chapman, I. T., Walkden, N. R., Graves, J. P. & Wahlberg, C. 2011 The effects of sheared toroidal rotation on stability limits in tokamak plasmas. *Plasma Phys. Control. Fusion* **53** (12), 125002.

Chu, M. S. 1998 Shear flow destabilization of a slowly rotating tokamak. *Phys. Plasmas* **5** (1), 183–191.

Chu, M. S., Greene, J. M., Jensen, T. H., Miller, R. L., Bondeson, A., Johnson, R. W. & Mauel, M. E. 1995 Effect of toroidal plasma flow and flow shear on global magnetohydrodynamic MHD modes. *Phys. Plasmas* **2** (6), 2236–2241.

Cooper, W. A. 1988 Ballooning instabilities in tokamaks with sheared toroidal flows. *Plasma Phys. Control. Fusion* **30** (13), 1805–1812.

https://doi.org/10.1017/S0022377820001178 Published online by Cambridge University Press

DLMF 2020 NIST Digital library of mathematical functions. http://dlmf.nist.gov/ Release 1.0.26 of 2020-03-15.

Eriksson, L.-G., Righi, E. & Zastrow, K.-D. 1997 Toroidal rotation in ICRF-heated H-modes on JET. *Plasma Phys. Control. Fusion* **39** (1), 27–42.

Fitzpatrick, R. 2008 A sharp boundary model for the vertical and kink stability of large aspect-ratio vertically elongated tokamak plasmas. *Phys. Plasmas* **15** (9), 092502.

Fitzpatrick, R. & Aydemir, A. Y. 1996 Stabilization of the resistive shell mode in tokamaks. *Nucl. Fusion* **36** (1), 11–38.

Freidberg, J. P. 2007 *Plasma Physics and Fusion Energy*. Cambridge University Press.

Freidberg, J. P. 2014 *Ideal MHD*. Cambridge University Press.

Freidberg, J. P. & Grossmann, W. 1975 Magnetohydrodynamic stability of a sharp boundary model of tokamak. *Phys. Fluids* **18** (11), 1494–1506.

Freidberg, J. P. & Haas, F. A. 1973 Kink instabilities in a high-β tokamak. *Phys. Fluids* **16** (11), 1909–1916.

Freidberg, J. P. & Haas, F. A. 1974 Kink instabilities in a high-β tokamak with elliptic cross section. *Phys. Fluids* **17**, 440.

Frieman, E. & Rotenberg, M. 1960 On hydromagnetic stability of stationary equilibria. *Rev. Mod. Phys*. **32**, 898–902.

Goedbloed, J. P. 1982 Free-boundary high-beta tokamaks. III. Free-boundary stability. *Phys. Fluids* **25** (11), 2073–2088.

Goedbloed, J. P., Keppens, R. & Poedts, S. 2010 *Advanced Magnetohydrodynamics*. Cambridge University Press.

Guazzotto, L., Freidberg, J. P. & Betti, R. 2008 A general formulation of magnetohydrodynamic stability including flow and a resistive wall. *Phys. Plasmas* **15** (7), 072503.

Hameiri, E. 1983 The equilibrium and stability of rotating plasmas. *Phys. Fluids* **26** (1), 230–237.

Hassam, A. B. & Kulsrud, R. M. 1978 Time evolution of mass flows in a collisional tokamak. *Phys. Fluids* **21** (12), 2271–2279.

Hazeltine, R. D. & Meiss, J. D. 2003 *Plasma Confinement*. Dover.

Hinton, F. L. & Wong, S. K. 1985 Neoclassical ion transport in rotating axisymmetric plasmas. *Phys. Fluids* **28** (10), 3082–3098.

Ito, A. & Nakajima, N. 2019 Magnetic flux coordinates for analytic high-beta tokamak equilibria with flow. *Plasma Phys. Control. Fusion* **61** (10), 105006.

Lee, J. & Cerfon, A. 2019 Magnetic shear due to localized toroidal flow shear in tokamaks. *Plasma Phys. Control. Fusion* **61** (10), 105007.

López, O. E. & Guazzotto, L. 2017 High-beta analytic equilibria in circular, elliptical, and D-shaped large aspect ratio axisymmetric configurations with poloidal and toroidal flows. *Phys. Plasmas* **24** (3), 032501.

Morris, R. C., Haines, M. G. & Hastie, R. J. 1996 The neoclassical theory of poloidal flow damping in a tokamak. *Phys. Plasmas* **3** (12), 4513–4520.

Rhodes, D. J., Cole, A. J., Brennan, D. P., Finn, J. M., Li, M., Fitzpatrick, R., Mauel, M. E. & Navratil, G. A. 2018 Shaping effects on toroidal magnetohydrodynamic modes in the presence of plasma and wall resistivity. *Phys. Plasmas* **25** (1), 012517.

Sabbagh, S. A., Sontag, A. C., Bialek, J. M., Gates, D. A., Glasser, A. H., Menard, J. E., Zhu, W., Bell, M. G., Bell, R. E., Bondeson, A., *et al.* 2006 Resistive wall stabilized operation in rotating high beta NSTX plasmas. *Nucl. Fusion* **46** (5), 635–644.

Shumlak, U. & Hartman, C. W. 1995 Sheared flow stabilization of the $m = 1$ kink mode in Z pinches. *Phys. Rev. Lett*. **75**, 3285–3288.

Solov'ev, L. S. 1968 The theory of hydromagnetic stability of toroidal plasma configurations. *Sov. Phys. JETP* **26**, 400–407.

Suckewer, S., Eubank, H. P., Goldston, R. J., McEnerney, J., Sauthoff, N. R. & Towner, H. H. 1981 Toroidal plasma rotation in the PLT tokamak with neutral-beam injection. *Nucl. Fusion* **21** (10), 1301–1309.

Waelbroeck, F. L. 1996 Gyroscopic stabilization of the internal kink mode. *Phys. Plasmas* **3** (3), 1047–1053.

https://doi.org/10.1017/S0022377820001178 Published online by Cambridge University Press

WAELBROECK, F. L. & CHEN, L. 1991 Ballooning instabilities in tokamaks with sheared toroidal flows. *Phys. Fluids* B **3** (3), 601–610.

WAHLBERG, C. & BONDESON, A. 1997 Stability analysis of the ideal $m = n = 1$ kink mode in toroidal geometry by direct expansion of the hydromagnetic equations. *J. Plasma Phys*. **57** (2), 327–341.

WAHLBERG, C. & BONDESON, A. 2000 Stabilization of the internal kink mode in a tokamak by toroidal plasma rotation. *Phys. Plasmas* **7** (3), 923–930.

WAHLBERG, C. & BONDESON, A. 2001 Stabilization of the mercier modes in a tokamak by toroidal plasma rotation. *Phys. Plasmas* **8** (8), 3595–3604.

WAHLBERG, C., CHAPMAN, I. T. & GRAVES, J. P. 2009 Importance of centrifugal effects for the internal kink mode stability in toroidally rotating tokamak plasmas. *Phys. Plasmas* **16** (11), 112512.

WAHLBERG, C., GRAVES, J. P. & CHAPMAN, I. T. 2013 Analysis of global hydromagnetic instabilities driven by strongly sheared toroidal flows in tokamak plasmas. *Plasma Phys. Control. Fusion* **55** (10), 105004.

https://doi.org/10.1017/S0022377820001178 Published online by Cambridge University Press